

pubs.acs.org/JPCC Article

Vibrational Mode Assignment of Diisopropyl Benzimidazolium N-Heterocyclic Carbenes on Gold

Published as part of The Journal of Physical Chemistry C virtual special issue "Celebrating 50 Years of Surface Enhanced Spectroscopy".

Shayanta Chowdhury, Gaohe Hu, Isabel M. Jensen, Alyssa V. B. Santos, David M. Jenkins,* Lasse Jensen,* and Jon P. Camden*



Cite This: J. Phys. Chem. C 2024, 128, 13550-13557



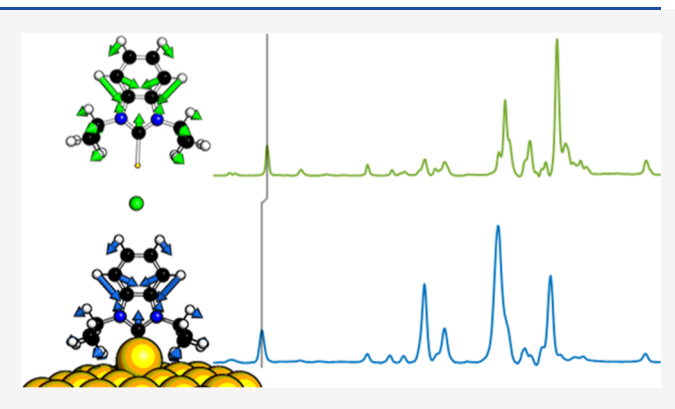
ACCESS I

Metrics & More

Article Recommendations

Supporting Information

ABSTRACT: Raman, surface-enhanced Raman, and infrared vibrational spectra of diisopropyl benzimidazolium N-heterocyclic carbenes were experimentally measured and calculated using firstprinciples theory. Experimental data were in excellent agreement with the theory and allowed for assignment of previously unreported vibrational modes in the molecule. Key vibrational motions of the Au-C bond, benzene ring, and isopropyl wingtips were isolated using ¹³C-labeled isotopes, and weighted SERS calculations reveal the specific characteristics of these motions in the SERS signatures.



INTRODUCTION

In recent years, N-heterocyclic carbene (NHC) ligands have emerged as thiol alternatives, utilizing strong sigma bonds to form well-defined, highly ordered self-assembled monolayers (SAMs) on transition metal surfaces and nanoparticles. ^{1–3} With the first reports of NHC-functionalized nanoparticles by Tilley and co-worker⁴ and Fairlamb and Chechik and co-workers⁵ and subsequent formative work by Crudden and co-workers,6 Johnson and co-workers, and Glorius and Ravoo and coworkers⁸ NHCs have been established as SAMs with excellent surface passivation and structural diversity, enabling applications in fields of biomedicine, catalysis, sensing, and molecular electronics. 12,13 NHCs were originally, and still continue to be, prized in organometallic chemistry for homogeneous catalysis applications. 14 Consequently, there are many works focusing on the spectroscopic characterization of NHCs including benzimidazolium salts, 15,16 imidazolium salts, 17 free carbene moieties, 18 and CO₂ adducts. 19

Vibrational spectroscopies such as high-resolution electron energy loss spectroscopy (HREELS), 11,20 surface-enhanced Raman spectroscopy (SERS), ^{21,22} and reflection absorption infrared (IR) spectroscopy (RAIRS)^{23,24} have been applied as a tool to study NHC SAMs. They are often used to monitor monolayer formation and stability, 24,25 surface chemical reactions, ^{26,27} and catalysis. ^{28,29} While previous studies have reported on a subset of the imidazolium and benzimidazolium NHC vibrational modes, 11,30 a systematic and rigorous vibrational mode analysis of NHCs bound to gold is missing in the literature. This absence is likely due to the complexity arising from the NHC being bonded to the metal surface and from the coupling of ring modes, isopropyl wingtip modes, and carbene-metal modes in the molecule.

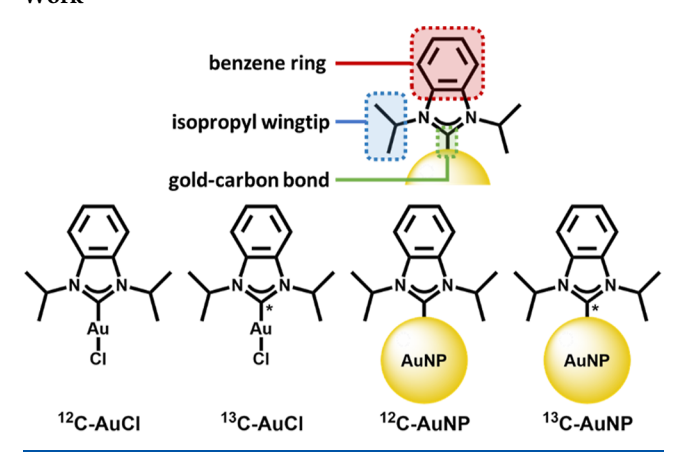
In this paper, we focus on the well-studied diisopropyl benzimidazolium NHC and its ¹³C-labeled isotopologue, both as a gold(I) chloride salt and as a ligand bound to gold nanoparticles (Scheme 1). Table S1 provides a comprehensive view of previous studies reporting on vibrational modes of NHCs bound to various flat metal surfaces, with descriptions of the modes assigned by the authors. 11,20,23,24 This survey is the starting point for the current study, although it is necessary to realize that detailed normal mode coordinates are not always reported in these previous studies. Prior work by our group using SERS to study NHCs on gold nanoparticles has focused specifically on normal modes with Au-C character.³¹ The diisopropyl benzimidazolium NHC complex has C_{2v} symmetry and, as such, possesses some normal modes that are only Ramanactive or only IR-active. Given the complexity of the molecular

Received: April 4, 2024 Revised: July 26, 2024 Accepted: July 29, 2024 Published: August 6, 2024





Scheme 1. Structures of NHC Gold(I) Complexes and Gold Nanoparticles Functionalized with NHCs Examined in This Work



structure, we additionally expect many vibrational bands to overlap, which complicates the interpretation and identification of specific spectral features utilizing group theory alone. Thus, to understand the spectra, we compare experimental measurements of the Raman, SERS, and IR spectra of the two isotopologues to first-principles theory calculations, which allows us to assign previously unreported vibrational modes. Further analysis of the weighted character of motions of the wingtip, benzene ring, and gold—carbon stretch provides a deeper understanding of the constituents of these normal modes.

METHODS

The synthesis of 1,3-diisopropyl benzimidazolium gold(I) chloride and the corresponding ¹³C labeling of the carbene carbon were done according to previously published protocols. ^{30,31} Scheme 1 summarizes the naming convention of the resulting complexes and nanoparticles used throughout this paper. A top-down ligand exchange method ²⁶ was used to functionalize 60 nm quasi-spherical citrate-capped AuNPs with both the naturally abundant and ¹³C-labeled complexes.

Previous work by our group has shown that the SERS spectra are invariant over a range of different sizes of AuNPs from 20 to 100 nm. ²⁶

The ATR-FTIR spectra of the neat powders of $^{12}C-AuCl$ and $^{13}C-AuCl$ were measured on a Thermo Scientific Nicolet iS10, with a Smart iTR accessory. 10 mM solutions of $^{12}C-AuCl$ and $^{13}C-AuCl$ dissolved in CH_2Cl_2 were drop-casted on a clean glass slide and left to evaporate under ambient conditions for Raman measurements. The Raman spectra were taken on a custom-built setup using 633 nm excitation by focusing the laser on the dried sample with a $20\times$ Nikon objective (NA = 0.5) in an inverted Nikon Eclipse Ti–U microscope. The SERS spectra were measured in the same setup by focusing on self-aggregated clusters of $^{12}C-AuNP$ and $^{13}C-AuNP$.

To assign the vibrational modes observed experimentally, the spectra were compared to calculations obtained from a local version of the Amsterdam Density Functional (ADF) engine from Amsterdam Modeling Suite. Service Servi

Modeling of SERS of NHCs on gold nanoparticles was done assuming a strong local field enhancement perpendicular to the surface such that only contributions from the Raman tensor along the local field were included. This ensures that the SERS surface-selection rules are obeyed. Chemical effects were included by including a small metal cluster in the calculations. This approach neglects the coupling between the chemical and electromagnetic effects. For the NHCs studied in this work, this is a reasonable approximation due to the strong binding of the NHCs through an adatom. An AuS8 cluster with an adatom was chosen to ensure a large enough cluster to support the wingtips of NHCs in a flat configuration. Previous work using

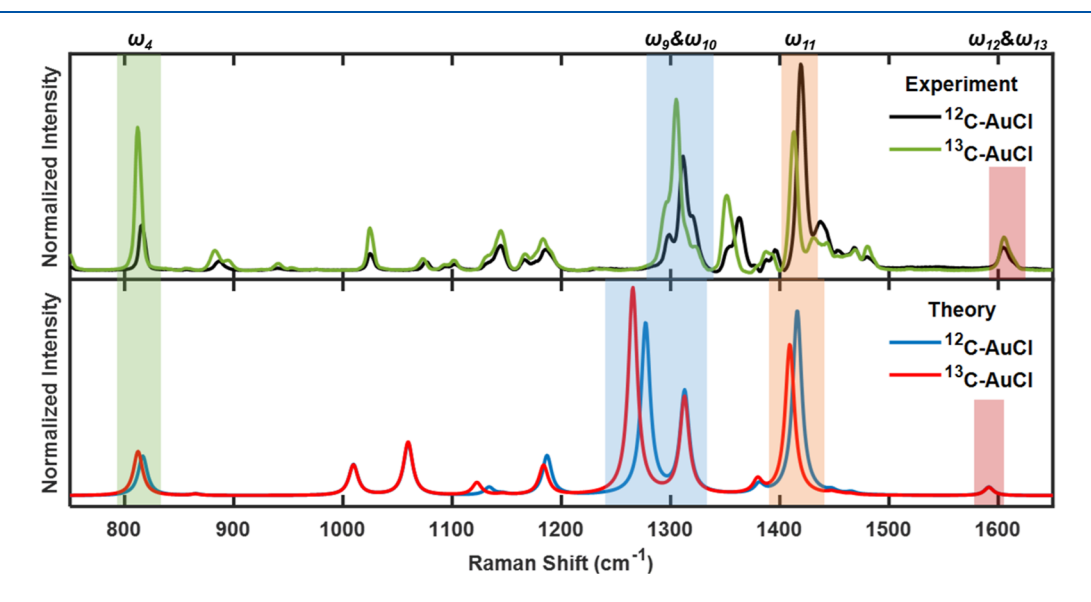


Figure 1. Experimental (top) and theoretical (bottom) Raman spectra of NHC gold complexes 12 C-AuCl and 13 C-AuCl. The assigned modes ω_4 , $\omega_9 \& \omega_{10}$, ω_{11} , and $\omega_{12} \& \omega_{13}$ are highlighted in green, blue, orange, and red, respectively.

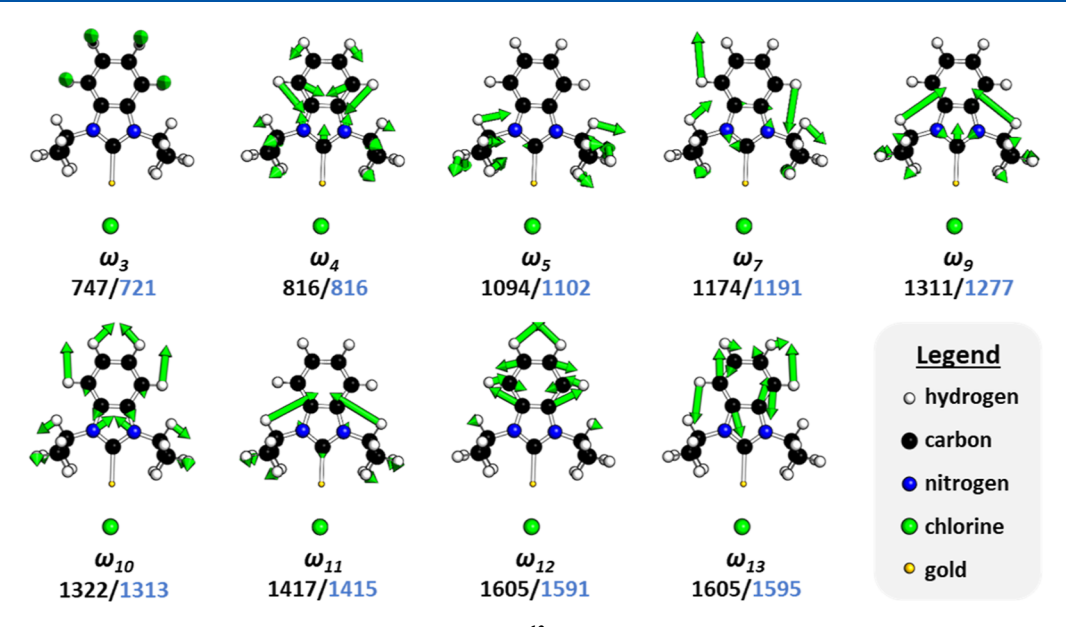


Figure 2. Normal mode images of assigned Raman and IR active modes of 12 C-AuCl. The experimental and calculated frequencies are denoted below the modes in units of cm $^{-1}$, with experimental values in black and calculated values in blue.

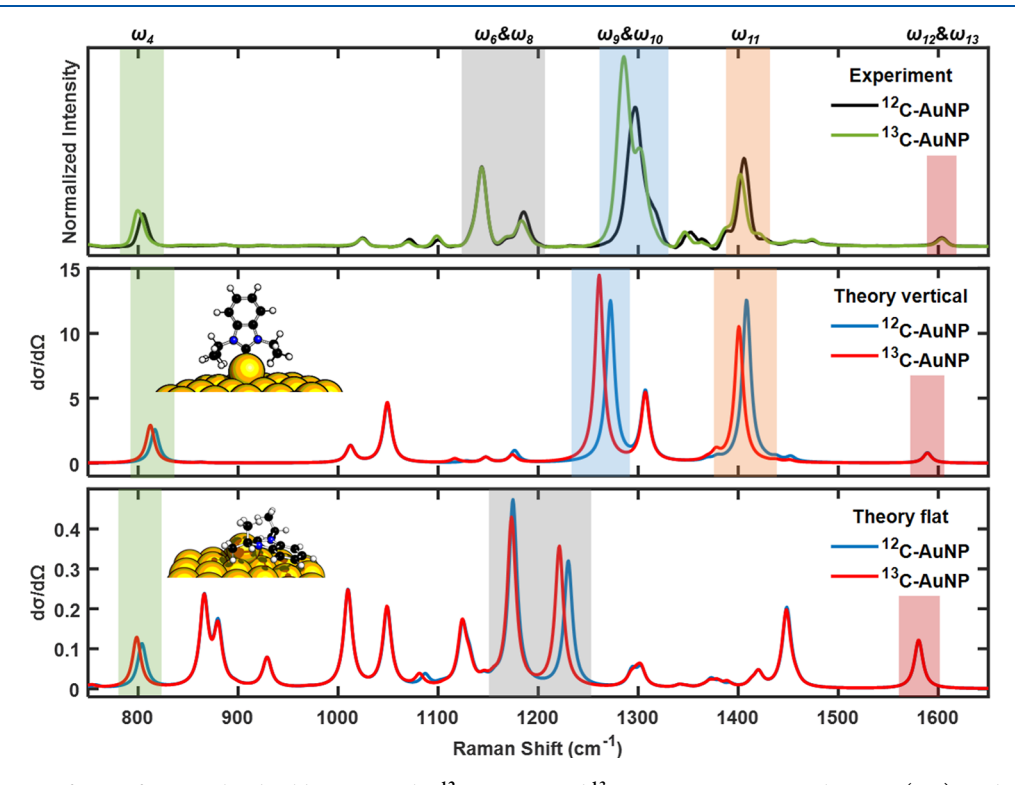


Figure 3. SERS spectra of NHC-functionalized gold nanoparticles 12 C-AuNP and 13 C-AuNP. Experimental spectra (top) can be interpreted with a combination of the vertical (middle) and flat (bottom) orientations of the NHCs on the gold cluster. The assigned modes $ω_4$, $ω_6$ & $ω_8$, $ω_9$, $ω_{11}$, and $ω_{12}$ & $ω_{13}$ are highlighted in green, gray, blue, orange, and red, respectively. The theoretical Raman cross section (d σ /d Ω) for the theory plots is in units of 10^{-30} cm 2 sr $^{-1}$.

this cluster model has shown good agreement with experimental SERS spectra. ^{22,30} For all calculations, the BP86 XC functional was chosen because predicted vibrational frequencies are typically in good agreement with experimental frequencies without the need for a scale factor. ⁴¹ Additionally, a mobile block Hessian was used to decouple the vibrational motions of Au atoms in the cluster with molecular vibrations. In this way, low-frequency vibration motions such as Au–Au stretching motions are eliminated from the simulated spectra. The low-

frequency vibrational modes are often very anharmonic and are therefore difficult to assign. For this reason, the assignment of new modes was limited to the range of 750–1650 cm⁻¹. Further details of the synthesis procedure and subsequent characterizations and computational analysis can be found in the Supporting Information.

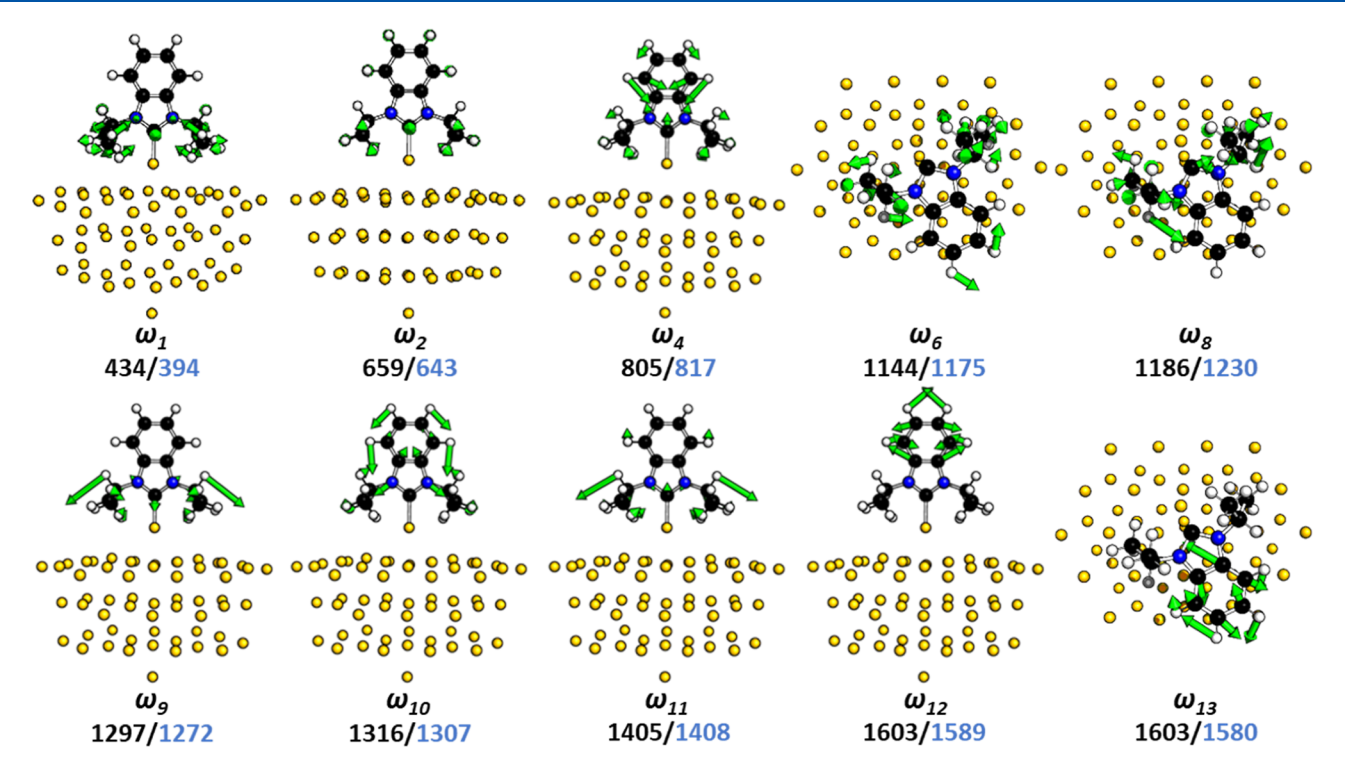


Figure 4. Normal mode images of assigned SERS active modes. The experimental and calculated frequencies are denoted below the modes in units of cm⁻¹, with experimental values in black and calculated values in blue.

RESULTS AND DISCUSSION

We begin by exploring the 750-1650 cm⁻¹ region, where the strongest Raman signatures are obtained; however, this region also has multiple overlapping bands. Figure 1 compares the experimental neat Raman spectra and corresponding calculated spectra of ¹²C-AuCl and ¹³C-AuCl. The full wavenumber region of the experimental spectra is shown in Figure S4. The two strongest Raman signals occur in the experimental spectra at 1311 and 1417 cm⁻¹, with their corresponding calculated peaks at 1277 and 1415 cm⁻¹. Both modes show red shifts for ¹³C-AuCl, and they have comparable relative intensities for both isotopes. Hence, these are assigned the vibrational normal modes denoted as ω_9 and ω_{11} , respectively, comprising a mix of different wingtip motions and an Au-C stretch, as shown in Figure 2. ω_{10} has a calculated frequency of 1313 cm⁻¹ and does not contain significant Au-C motion, thus showing no red shift with the isotope. Deconvolution of the experimental cluster of peaks around 1300 cm $^{-1}$ reveals the ω_{10} mode to be a shoulder peak observed experimentally at 1322 cm⁻¹ and is further confirmed by its lack of an isotope shift (Figure S3). This mode may be correlated to the $\sim 1360 \text{ cm}^{-1}$ mode reported in prior studies (Table S1). The 816 cm⁻¹ peak, which does show an isotopic shift, is assigned to the normal mode ω_4 : a mixture of the Au-C stretch, ring in-plane symmetric stretch, and wingtip mode. Assignment of a Au-C stretch in this region is missing in previous reports, although we have found this mode to have one of the highest percentages of Au-C character.³¹ Finally, the 1605 cm⁻¹ peak in the experimental spectra is assigned to the degenerate modes ω_{12} and ω_{13} , corresponding to ring in-plane symmetric stretches and asymmetric stretches of the benzene ring, respectively. Benzimidazoles are known to show similar stretches of the benzene ring. 16 This is a well-reported ~1615 cm⁻¹ mode on flat metal surfaces, described to possess multiple ring vibrations (Table S1). This assignment is also consistent

with our previous study of the effect of deuteration of wingtips to the SERS of NHCs, which showed no shift in this mode with deuteration.³⁰

We extend our analysis to surface-bound NHCs by recording the SERS spectra of 12C-AuNP and 13C-AuNP which are shown in Figure 3. The normal modes in the Raman analysis are all found to have direct counterparts in the SERS spectrum, where they are slightly shifted to lower wavenumbers. The surface enhancement provides a significant boost in signal intensity but adds complexity because of its preferential enhancement of vibrations perpendicular to the surface of the metal. 42,43 Hotspot dependence of SERS enhancement is a wellreported phenomenon, and care needs to be taken when analyzing low concentration or single molecules quantitatively. 44,45 Previous work by our group has shown SERS to be a robust technique in providing a consistent picture of NHC binding on gold, as evidenced by agreement with other techniques that do not preferentially utilize hotspots, such as HREELS.²¹ Additionally, NHC ligands bind as an adatom on gold with an upright or a flat orientation (or really any other angle in between) depending on the packing on the surface, as shown by multiple groups using various techniques.^{20,46–49} Recent work by our group has shown that each of these orientations has their unique SERS signatures. 22 To circumvent this issue, we consider the theoretical spectra of our NHC molecule as if it was only flat and only vertical independently as two different spectra and then examine the experimental spectra as a combination of the two. While this simplifies the analysis, we do not consider any angles between the flat and vertical orientations, which likely oversimplifies the actual orientation due to the bulk of the isopropyl wingtips.

Despite this issue, the enhancement in intensity allowed us to make two additional mode assignments. The pair of experimental peaks highlighted in gray (1120–1200 cm⁻¹) in Figure 3 has comparable peaks in the calculated spectra when we

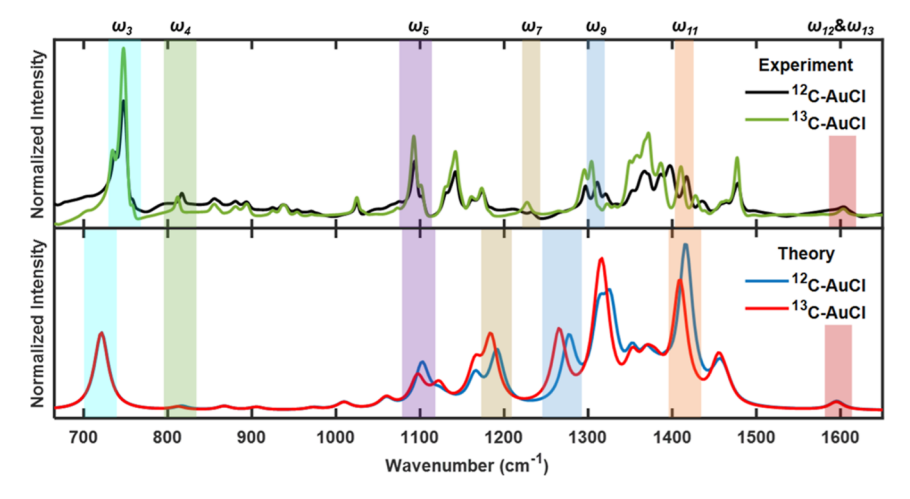


Figure 5. Experimental (top) and calculated (bottom) ATR-FTIR spectra of NHC gold complexes 12 C-AuCl and 13 C-AuCl. The assigned modes ω_3 , ω_4 , ω_5 , ω_7 , ω_9 , ω_{11} , and ω_{12} & ω_{13} are highlighted in cyan, green, violet, brown, blue, orange, and red, respectively.

consider their placement, relative intensity, and isotope shifts. The experimental peak at 1144 cm⁻¹ does not shift, and is assigned as ω_6 , which is seen to consist of wingtip motion of the flat molecule coupled to in-plane bending of part of the benzene ring, with no Au-C vibration, as shown in Figure 4. This mode may be the previously reported mode at ~1155 cm⁻¹ with wingtip and aromatic CH vibrations for the diisopropyl benzimidazolium NHC on flat metal surfaces (Table S1). The experimental 1186 cm⁻¹ peak is assigned as ω_8 whose motion couples the wingtip motion and the Au-C motion, evident by the isotope shift of this mode. The much lower intensity of these two peaks compared to the ω_9 peak highlighted in blue makes sense when we compare the Raman cross sections $(d\sigma/d\Omega)$ on the y axis. The highest signal for the vertical orientation spectra is 30× stronger than the highest signal in the flat orientation spectra. The Raman mode ω_{10} is difficult to pinpoint in the SERS spectra and is likely hidden in the cluster of peaks in the 1300 cm⁻¹ region. We also see isotopic red shifts in the same bands at 804, 1297, and 1405 cm⁻¹, which reconfirm our assignments in the Raman spectra.

Figure 5 shows the IR spectra of complexes 12 C-AuCl and 13 C-AuCl. Again, some of the normal modes from Raman and SERS are present in the IR, i.e., ω_4 , ω_9 , ω_{11} , and ω_{12} & ω_{13} . The intense peak at 747 cm⁻¹ shows no shift, but peaks at 816, 1094, 1174, 1311, and 1417 cm⁻¹ do show red shifting due to isotope labeling. This allows for the identification of three more modes that are only IR-active: ω_3 , ω_5 , and ω_7 . These modes are all asymmetric stretches. The specific motions of the atoms in the normal mode images shown in Figure 2 verify that these vibrations change the dipole moment of the molecule with no change in the polarizability, resulting in only IR active modes. ω_3 has been reported in HREELS and RAIRS to consist of out-of-plane aromatic CH vibrations at ~750 cm⁻¹. 11,23 Table 1 summarizes the experimental IR, Raman, and SERS vibrations and their complementary theoretical peak positions.

After assigning the modes of the major peaks in each of the spectra discussed above, we investigate the contribution of the different motions that form the basis of each normal mode image. To isolate the isopropyl wingtip, benzene ring, and Au–C vibrations in the modes, we theoretically determine the weighted SERS of each of these motions. The weighted SERS spectra are calculated by scaling the original SERS intensity by a mode composition factor. ⁵⁰ The mode composition factor (shown in

Table 1. Vibrational Modes of Diisopropyl Benzimidazolium NHC^a

$v_{\rm IR}~({\rm cm}^{-1})$		$v_{\rm Raman}$ (cm ⁻¹)		$\nu_{\rm SERS}~({\rm cm}^{-1})$		vibrational assignment
expt	theory	expt	theory	expt	theory	
				434	394	ω_1
				659	643	ω_2
747	721					ω_3
816	816	816	816	805	817	ω_4
1094	1102					ω_5
				1144	1175	ω_6
1174	1191					ω_7
				1186	1230	ω_8
1311	1277	1311	1277	1297	1272	ω_9
		1322sh	1313	1316sh	1307	ω_{10}
1417	1415	1419	1415	1405	1408	ω_{11}
1603	1591	1605	1591	1603	1589	ω_{12}
1603	1595	1605	1595	1603	1580	ω_{13}

^aExperimental and calculated IR, Raman, and SERS frequencies of the modes assigned in this study. sh: shoulder peak.

eq 1) determines the contribution from each of the atoms to a certain normal mode where m_i is the atomic mass and r_i is the atomic displacement for that mode. For a certain region of the system, such as the wingtip, the original Raman is scaled by summation of mode composition factors in this region for each mode, respectively.

$$f_j = \frac{m_j r_j^2}{\sum_i m_i r_i^2} \tag{1}$$

Figure S6 visualizes the results of this analysis as a bar plot for the flat and vertical orientations of the NHC on the gold cluster. The y axis represents the percentage of the total intensity of the normal mode that can be attributed to the isolated vibration. The color map represents the calculated total intensity of the normal modes in question. Only the modes assigned in this study have been shown in the figure for simplicity. Importantly, our previous assignments of the vibrational character can be verified by looking at the specific frequency regions. For example, the green shade representing the 816 cm^{-1} (ω_4) mode shows mainly a mixture of Au–C and ring vibration, and the

 $1603~{\rm cm}^{-1}~(\omega_{12})$ mode shaded in red is almost entirely ring motion.

Until now, for ease of mode assignment, we discussed only the side-down wingtip orientation in the theory calculations. The frequency region below 800 cm⁻¹ is comprised of mainly ring and wingtip vibrations, but these can show variation with wingtip substituents, as evident in the SERS reported in our wingtip-dependent orientation study.²² This trait is also observed in imidazolium salts with similar structures.¹⁷ Below 800 cm⁻¹, the up/down configuration becomes significant when considering the weighted SERS of the wingtips, as can be seen in Figure S7H and I. This can be attributed to the increased SERS enhancement as one approaches the surface. For other bands, the weighted SERS of the benzene ring and the Au-C bond is not dependent on wingtip configuration, which allowed us to assign two unique modes in our previous Au-C bond study: the 434 cm⁻¹ mode is assigned ω_1 with Au–C vibration coupled to wingtip motions and the 659 cm⁻¹ mode ω_2 with out-of-plane motions in the benzene ring coupled to both wingtip and Au-C motion.³¹ Previous reports assign the metal-carbene stretch of NHCs on surfaces in the $420-430 \text{ cm}^{-1}$ region, while the ~ 650 cm⁻¹ mode is assigned a ring stretch (Table S1). Through this analysis, we are able to get a more complete picture of these normal modes and can conclude that they have significant Au-C character (Figure S6). Below 400 cm⁻¹, wingtip character completely dominates the spectra (Figure S7) but is harder to interpret due to the low intensity of the peaks and the effects of anharmonicity.

CONCLUSIONS

In this paper, we compare experimentally measured Raman and IR vibrational spectra of a model NHC with theoretically calculated spectra for a set of isotopically labeled compounds. Using this comparison, we can identify several previously unassigned modes, allowing us to attain a more comprehensive picture of the normal modes associated with the IR, Raman, and SERS bands. While a complete description of all NHC vibrational modes is not possible due to overlapping bands or low-intensity peaks, we report detailed mode assignments of 13 modes in this paper, three of which are only IR-active. Weighted SERS calculations additionally allow us to verify the vibrational character of these band assignments and discern the dominant character of the normal modes in specific regions.

ASSOCIATED CONTENT

Supporting Information

The Supporting Information is available free of charge at https://pubs.acs.org/doi/10.1021/acs.jpcc.4c02228.

List of previously reported mode assignments, details of synthesis procedures, instrumentation, computational analysis, additional spectra, table of vibrational mode images, and weighted SERS plots (PDF)

Coordinate files of optimized geometries of NHCs on gold (ZIP)

AUTHOR INFORMATION

Corresponding Authors

David M. Jenkins — Department of Chemistry, The University of Tennessee, Knoxville, Tennessee 37996, United States; orcid.org/0000-0003-2683-9157; Email: jenkins@ion.chem.utk.edu

Lasse Jensen — Department of Chemistry, The Pennsylvania State University, University Park, Pennsylvania 16802, United States; orcid.org/0000-0003-1237-5021; Email: jensen@chem.psu.edu

Jon P. Camden — Department of Chemistry and Biochemistry, University of Notre Dame, Notre Dame, Indiana 46556, United States; orcid.org/0000-0002-6179-2692; Email: jon.camden@nd.edu

Authors

Shayanta Chowdhury — Department of Chemistry and Biochemistry, University of Notre Dame, Notre Dame, Indiana 46556, United States; Occid.org/0000-0002-0878-4781

Gaohe Hu – Department of Chemistry, The Pennsylvania State University, University Park, Pennsylvania 16802, United States

Isabel M. Jensen – Department of Chemistry, The University of Tennessee, Knoxville, Tennessee 37996, United States

Alyssa V. B. Santos — Department of Chemistry, The Pennsylvania State University, University Park, Pennsylvania 16802, United States; Present Address: Department of Chemistry, St. Bonaventure University, St. Bonaventure, New York 14778, USA; orcid.org/0000-0002-7501-5819

Complete contact information is available at: https://pubs.acs.org/10.1021/acs.jpcc.4c02228

Author Contributions

[⊥]S.C. and G.H. contributed equally. S.C. and G.H. wrote the manuscript. G.H. and A.V.B.S. contributed to the theory calculations. S.C. performed Raman and SERS. I.M.J. synthesized the complexes and contributed the IR.

Funding

CHE-2108330 (S.C. and J.P.C.), CHE-2312222 (G.H. and L.J.), CHE-2108328 (I.M.J. and D.M.J.), and DGE 1255832 (A.V.B.S).

Notes

The authors declare no competing financial interest.

ACKNOWLEDGMENTS

This material is based upon the work supported by the National Science Foundation under grant numbers CHE-2108330 (S.C. and J.P.C.), CHE-2312222 (G.H. and L.J.), CHE-2108328 (I.M.J. and D.M.J.), and DGE 1255832 (A.V.B.S.).

ABBREVIATIONS

NHC, N-heterocyclic carbene; SAM, self-assembled monolayer; HREELS, high-resolution electron energy loss spectroscopy; SERS, surface-enhanced Raman spectroscopy; RAIRS, reflection absorption infrared spectroscopy; AuNP, gold nanoparticle; ADF, Amsterdam density functional; ATR-FTIR, attenuated total reflectance Fourier transform infrared.

REFERENCES

- (1) Smith, C. A.; Narouz, M. R.; Lummis, P. A.; Singh, I.; Nazemi, A.; Li, C. H.; Crudden, C. M. N. N-Heterocyclic Carbenes in Materials Chemistry. *Chem. Rev.* **2019**, *119* (8), 4986–5056.
- (2) Bellotti, P.; Koy, M.; Hopkinson, M. N.; Glorius, F. Recent advances in the chemistry and applications of *N*-heterocyclic carbenes. *Nat. Rev. Chem* **2021**, *5* (10), 711–725.
- (3) Kaur, G.; Thimes, R. L.; Camden, J. P.; Jenkins, D. M. Fundamentals and applications of N-heterocyclic carbene function-

- alized gold surfaces and nanoparticles. Chem. Commun. 2022, 58 (95), 13188-13197.
- (4) Vignolle, J.; Tilley, T. D. *N*-Heterocyclic carbene-stabilized gold nanoparticles and their assembly into 3D superlattices. *Chem. Commun.* **2009**, No. 46, 7230–7232.
- (5) Hurst, E. C.; Wilson, K.; Fairlamb, I. J. S.; Chechik, V. N-Heterocyclic carbene coated metal nanoparticles. *New J. Chem.* **2009**, 33 (9), 1837–1840.
- (6) Crudden, C. M.; Horton, J. H.; Ebralidze, I. I.; Zenkina, O. V.; McLean, A. B.; Drevniok, B.; She, Z.; Kraatz, H. B.; Mosey, N. J.; Seki, T.; et al. Ultra stable self-assembled monolayers of *N*-heterocyclic carbenes on gold. *Nat. Chem.* **2014**, *6* (5), 409–414.
- (7) Zhukhovitskiy, A. V.; Mavros, M. G.; Van Voorhis, T.; Johnson, J. A. Addressable carbene anchors for gold surfaces. *J. Am. Chem. Soc.* **2013**, *135* (20), 7418–7421.
- (8) Richter, C.; Schaepe, K.; Glorius, F.; Ravoo, B. J. Tailor-made *N*-heterocyclic carbenes for nanoparticle stabilization. *Chem. Commun.* (*Camb*) **2014**, *50* (24), 3204–3207.
- (9) Thomas, S. R.; Casini, A. N. N-Heterocyclic carbenes as "smart" gold nanoparticle stabilizers: State-of-the art and perspectives for biomedical applications. *J. Organomet. Chem.* **2021**, 938, 121743.
- (10) Koy, M.; Bellotti, P.; Das, M.; Glorius, F. N. N-Heterocyclic carbenes as tunable ligands for catalytic metal surfaces. *Nat. Catal.* **2021**, *4* (5), 352–363.
- (11) Crudden, C. M.; Horton, J. H.; Narouz, M. R.; Li, Z.; Smith, C. A.; Munro, K.; Baddeley, C. J.; Larrea, C. R.; Drevniok, B.; Thanabalasingam, B.; et al. Simple direct formation of self-assembled *N*-heterocyclic carbene monolayers on gold and their application in biosensing. *Nat. Commun.* **2016**, *7*, 12654.
- (12) Nguyen, D. T.; Freitag, M.; Korsgen, M.; Lamping, S.; Ruhling, A.; Schafer, A. H.; Siekman, M. H.; Arlinghaus, H. F.; van der Wiel, W. G.; Glorius, F.; et al. Versatile Micropatterns of *N*-Heterocyclic Carbenes on Gold Surfaces: Increased Thermal and Pattern Stability with Enhanced Conductivity. *Angew. Chem., Int. Ed. Engl.* **2018**, *57* (35), 11465–11469.
- (13) Kang, S.; Byeon, S. E.; Yoon, H. J. N-Heterocyclic Carbene Anchors in Electronics Applications. *Bull. Korean Chem. Soc.* **2021**, 42 (5), 712–723.
- (14) Hopkinson, M. N.; Richter, C.; Schedler, M.; Glorius, F. An overview of *N*-heterocyclic carbenes. *Nature* **2014**, *510* (7506), 485–496.
- (15) Malek, K.; Puc, A.; Schroeder, G.; Rybachenko, V. I.; Proniewicz, L. M. FT-IR and FT-Raman spectroscopies and DFT modelling of benzimidazolium salts. *Chem. Phys.* **2006**, *327* (2–3), 439–451.
- (16) Morsy, M. A.; Al-Khaldi, M. A.; Suwaiyan, A. Normal Vibrational Mode Analysis and Assignment of Benzimidazole by ab Initio and Density Functional Calculations and Polarized Infrared and Raman Spectroscopy. *J. Phys. Chem. A* **2002**, *106* (40), 9196–9203.
- (17) Paschoal, V. H.; Faria, L. F. O.; Ribeiro, M. C. C. Vibrational Spectroscopy of Ionic Liquids. *Chem. Rev.* **2017**, *117* (10), 7053–7112.
- (18) Talapaneni, S. N.; Buyukcakir, O.; Je, S. H.; Srinivasan, S.; Seo, Y.; Polychronopoulou, K.; Coskun, A. Nanoporous Polymers Incorporating Sterically Confined *N*-Heterocyclic Carbenes for Simultaneous CO2 Capture and Conversion at Ambient Pressure. *Chem. Mater.* **2015**, *27* (19), 6818–6826.
- (19) Zhou, H.; Zhang, W.-Z.; Liu, C.-H.; Qu, J.-P.; Lu, X.-B. CO₂ Adducts of *N*-Heterocyclic Carbenes: Thermal Stability and Catalytic Activity toward the Coupling of CO₂ with Epoxides. *J. Org. Chem.* **2008**, 73 (20), 8039–8044.
- (20) Larrea, C. R.; Baddeley, C. J.; Narouz, M. R.; Mosey, N. J.; Horton, J. H.; Crudden, C. M. N-Heterocyclic Carbene Self-assembled Monolayers on Copper and Gold: Dramatic Effect of Wingtip Groups on Binding, Orientation and Assembly. *ChemPhysChem* **2017**, *18* (24), 3536–3539.
- (21) DeJesus, J. F.; Trujillo, M. J.; Camden, J. P.; Jenkins, D. M. N-Heterocyclic Carbenes as a Robust Platform for Surface-Enhanced Raman Spectroscopy. J. Am. Chem. Soc. 2018, 140 (4), 1247–1250.
- (22) Thimes, R. L.; Santos, A. V. B.; Chen, R.; Kaur, G.; Jensen, L.; Jenkins, D. M.; Camden, J. P. Using Surface-Enhanced Raman

- Spectroscopy to Unravel the Wingtip-Dependent Orientation of *N*-Heterocyclic Carbenes on Gold Nanoparticles. *J. Phys. Chem. Lett.* **2023**, 14 (18), 4219–4224.
- (23) Zeng, Y.; Zhang, T.; Narouz, M. R.; Crudden, C. M.; McBreen, P. H. Generation and conversion of an *N*-heterocyclic carbene on Pt(111). *Chem. Commun.* **2018**, 54 (88), 12527–12530.
- (24) Zhang, T.; Khomane, S. B.; Singh, I.; Crudden, C. M.; McBreen, P. H. N-heterocyclic carbene adsorption states on Pt(111) and Ru(0001). Phys. Chem. Chem. Phys. 2024, 26 (5), 4083–4090.
- (25) Dominique, N. L.; Chandran, A.; Jensen, I. M.; Jenkins, D. M.; Camden, J. P. Unmasking the Electrochemical Stability of *N*-Heterocyclic Carbene Monolayers on Gold. *Chem. Eur. J.* **2024**, *30* (15), No. e202303681.
- (26) DeJesus, J. F.; Sherman, L. M.; Yohannan, D. J.; Becca, J. C.; Strausser, S. L.; Karger, L. F. P.; Jensen, L.; Jenkins, D. M.; Camden, J. P. A Benchtop Method for Appending Protic Functional Groups to *N*-Heterocyclic Carbene Protected Gold Nanoparticles. *Angew. Chem., Int. Ed. Engl.* **2020**, *59* (19), 7585–7590.
- (27) Berg, I.; Amit, E.; Hale, L.; Toste, F. D.; Gross, E. N. N-Heterocyclic Carbene Based Nanolayer for Copper Film Oxidation Mitigation. *Angew. Chem., Int. Ed.* **2022**, *61* (25), No. e202201093.
- (28) Cao, Z.; Kim, D.; Hong, D.; Yu, Y.; Xu, J.; Lin, S.; Wen, X.; Nichols, E. M.; Jeong, K.; Reimer, J. A.; et al. A Molecular Surface Functionalization Approach to Tuning Nanoparticle Electrocatalysts for Carbon Dioxide Reduction. *J. Am. Chem. Soc.* **2016**, *138* (26), 8120–8125.
- (29) Wu, C.-Y.; Wolf, W. J.; Levartovsky, Y.; Bechtel, H. A.; Martin, M. C.; Toste, F. D.; Gross, E. High-spatial-resolution mapping of catalytic reactions on single particles. *Nature* **2017**, *541* (7638), 511–515.
- (30) Trujillo, M. J.; Strausser, S. L.; Becca, J. C.; DeJesus, J. F.; Jensen, L.; Jenkins, D. M.; Camden, J. P. Using SERS To Understand the Binding of *N*-Heterocyclic Carbenes to Gold Surfaces. *J. Phys. Chem. Lett.* **2018**, *9* (23), 6779–6785.
- (31) Jensen, I. M.; Chowdhury, S.; Hu, G.; Jensen, L.; Camden, J. P.; Jenkins, D. M. Seeking a Au—C stretch on gold nanoparticles with ¹³C-labeled *N*-heterocyclic carbenes. *Chem. Commun.* **2023**, *59* (98), 14524–14527.
- (32) Te Velde, G.; Bickelhaupt, F. M.; Baerends, E. J.; Fonseca Guerra, C.; Van Gisbergen, S. J. A.; Snijders, J. G.; Ziegler, T. Chemistry with ADF. *J. Comput. Chem.* **2001**, 22 (9), 931–967.
- (33) Baerends, E. J.; Ziegler, T.; Atkins, A. J.; Autschbach, J.; Bashford, D.; Baseggio, O.; Bérces, A. *ADF 2021.204. SCM, Theoretical Chemistry*; Vrije Universiteit: Amsterdam, The Netherlands, 2021. http://www.scm.com.
- (34) Ghysels, A.; Van Neck, D.; Van Speybroeck, V.; Verstraelen, T.; Waroquier, M. Vibrational modes in partially optimized molecular systems. *J. Chem. Phys.* **2007**, *126* (22), 224102.
- (35) Ghysels, A.; Van Neck, D.; Waroquier, M. Cartesian formulation of the mobile block Hessian approach to vibrational analysis in partially optimized systems. *J. Chem. Phys.* **2007**, 127 (16), 164108.
- (36) Becke, A. D. Density-functional exchange-energy approximation with correct asymptotic behavior. *Phys. Rev. A* **1988**, 38 (6), 3098–3100
- (37) Perdew, J. P. Density-functional approximation for the correlation energy of the inhomogeneous electron gas. *Phys. Rev. B* **1986**, 33 (12), 8822–8824.
- (38) Grimme, S.; Ehrlich, S.; Goerigk, L. Effect of the damping function in dispersion corrected density functional theory. *J. Comput. Chem.* **2011**, 32 (7), 1456–1465.
- (39) The PyMOL Molecular Graphics System, Version 3.0; Schrödinger, LLC.
- (40) Chen, R.; Jensen, L. Quantifying the enhancement mechanisms of surface-enhanced Raman scattering using a Raman bond model. *J. Chem. Phys.* **2020**, *153* (22), 224704.
- (41) Neugebauer, J.; Hess, B. A. Fundamental vibrational frequencies of small polyatomic molecules from density-functional calculations and vibrational perturbation theory. *J. Chem. Phys.* **2003**, *118* (16), 7215–7225.

- (42) Langer, J.; Jimenez de Aberasturi, D.; Aizpurua, J.; Alvarez-Puebla, R. A.; Auguie, B.; Baumberg, J. J.; Bazan, G. C.; Bell, S. E. J.; Boisen, A.; Brolo, A. G.; et al. Present and Future of Surface-Enhanced Raman Scattering. *ACS Nano* **2020**, *14* (1), 28–117.
- (43) Moskovits, M.; Suh, J. S. Surface selection rules for surface-enhanced Raman spectroscopy: calculations and application to the surface-enhanced Raman spectrum of phthalazine on silver. *J. Phys. Chem.* **1984**, 88 (23), 5526–5530.
- (44) Fang, Y.; Seong, N.-H.; Dlott, D. D. Measurement of the Distribution of Site Enhancements in Surface-Enhanced Raman Scattering. *Science* **2008**, *321* (5887), 388–392.
- (45) Zrimsek, A. B.; Chiang, N.; Mattei, M.; Zaleski, S.; McAnally, M. O.; Chapman, C. T.; Henry, A.-I.; Schatz, G. C.; Van Duyne, R. P. Single-Molecule Chemistry with Surface- and Tip-Enhanced Raman Spectroscopy. *Chem. Rev.* **2017**, *117* (11), 7583–7613.
- (46) Wang, G.; Ruhling, A.; Amirjalayer, S.; Knor, M.; Ernst, J. B.; Richter, C.; Gao, H. J.; Timmer, A.; Gao, H. Y.; Doltsinis, N. L.; et al. Ballbot-type motion of N-heterocyclic carbenes on gold surfaces. *Nat. Chem.* **2017**, *9* (2), 152–156.
- (47) Bakker, A.; Timmer, A.; Kolodzeiski, E.; Freitag, M.; Gao, H. Y.; Mönig, H.; Amirjalayer, S.; Glorius, F.; Fuchs, H. Elucidating the Binding Modes of N-Heterocyclic Carbenes on a Gold Surface. *J. Am. Chem. Soc.* **2018**, *140* (38), 11889–11892.
- (48) Lovat, G.; Doud, E. A.; Lu, D.; Kladnik, G.; Inkpen, M. S.; Steigerwald, M. L.; Cvetko, D.; Hybertsen, M. S.; Morgante, A.; Roy, X.; et al. Determination of the structure and geometry of N-heterocyclic carbenes on Au(111) using high-resolution spectroscopy. *Chem. Sci.* **2019**, *10* (3), 930–935.
- (49) Dery, S.; Kim, S.; Tomaschun, G.; Haddad, D.; Cossaro, A.; Verdini, A.; Floreano, L.; Klüner, T.; Toste, F. D.; Gross, E. Flexible NO₂-Functionalized N-Heterocyclic Carbene Monolayers on Au (111) Surface. *Chem. Eur. J.* **2019**, 25 (66), 15067–15072.
- (50) Leu, B. M.; Zgierski, M. Z.; Wyllie, G. R. A.; Scheidt, W. R.; Sturhahn, W.; Alp, E. E.; Durbin, S. M.; Sage, J. T. Quantitative Vibrational Dynamics of Iron in Nitrosyl Porphyrins. *J. Am. Chem. Soc.* **2004**, *126* (13), 4211–4227.